Bioinspiration & Biomimetics

PAPER

Estimation of knee and ankle angles during walking using thigh and shank angles

To cite this article: Mahdy Eslamy and Arndt F Schilling 2021 *Bioinspir. Biomim.* **16** 066012

Bioinspiration & Biomimetics

CrossMark

RECEIVED
21 April 2021

REVISED
8 August 2021

ACCEPTED FOR PUBLICATION
7 September 2021

PUBLISHED
12 October 2021

PAPER

Estimation of knee and ankle angles during walking using thigh and shank angles

Mahdy Eslamy* and **Arndt F Schilling**

Applied Rehabilitation Technology ART Lab, Department for Trauma Surgery, Orthopaedics and Plastic Surgery, Universitätsmedizin Göttingen (UMG), 37075, Göttingen, Germany

* Author to whom any correspondence should be addressed.

E-mail: mahdy.eslamy@med.uni-goettingen.de and arndt.schilling@med.uni-goettingen.de

Keywords: estimation of knee angles, estimation of ankle angles, gait variable estimations, wavelets-based joint angle estimation

Abstract

Estimation of joints' trajectories is commonly used in human gait analysis, and in the development of motion planners and high-level controllers for prosthetics, orthotics, exoskeletons and humanoids. Human locomotion is the result of the cooperation between leg joints and limbs. This suggests the existence of underlying relationships between them which lead to a harmonic gait. In this study we aimed to estimate knee and ankle trajectories using thigh and shank angles. To do so, an estimation approach was developed that continuously mapped the inputs to the outputs, which did not require switching rules, speed estimation, gait percent identification or look-up tables. The estimation algorithm was based on a nonlinear auto-regressive model with exogenous inputs. The method was then combined with wavelets theory, and then the two were used in a neural network. To evaluate the estimation performance, three scenarios were developed which used only one source of inputs (i.e., only shank angles or only thigh angles). First, knee angles θ_k (outputs) were estimated using thigh angles θ_{th} (inputs). Second, ankle angles θ_a (outputs) were estimated using thigh angles θ_{sh} (inputs), and third, the ankle angles were estimated using shank angles (inputs). The proposed approach was investigated for 22 subjects at different walking speeds and the leave-one-subject-out procedure was used for training and testing the estimation algorithm. Average root mean square errors were 3.9°–5.3° and 2.1°–2.3° for knee and ankle angles, respectively. Average mean absolute errors (MAEs) MAEs were 3.2°–4° and 1.7°–1.8°, and average correlation coefficients ρ_{cc} were 0.95–0.98 and 0.94–0.96 for knee and ankle angles, respectively. The limitations and strengths of the proposed approach are discussed in detail and the results are compared with several studies.

1. Introduction

Human locomotion is the result of consecutive and synergistic cooperation between different joints and limbs of the lower extremities [1]. Estimation of the joints' angles is of interest in human gait studies [2, 3] and also in the development of motion planners for prosthetics, orthotics, exoskeletons [4–7], as well as humanoid robots [8, 9] and gait rehabilitation devices [10, 11]. Different methods have been proposed to estimate knee and ankle angular trajectories during human locomotion.

In echoing approach, the knee motions of the contralateral leg were used to estimate the subsequent knee motions of the other side [12, 13]. Problems of this method were the necessity to attach sensors to the contralateral side and the delayed replay of the previous step. In [14], complementary limb motion estimation was proposed and used together with principal component analysis [15] to overcome that problem. In this method, the state estimations were performed without delay, making it possible to react more efficiently to the environmental changes.

As a convention in gait biomechanics, a gait cycle starts with the heel contact and ends with the next heel contact of the same foot [2, 16]. The gait cycles are sometimes divided into 100 sections called gait percents. In [17] the ankle motions were predicted by estimating the gait percents and speeds. The shank angles and shank angular velocities were shifted and scaled to create quasi-circular curves when plotted together. Next, the angles between the points on the customized curve, the origin and the horizontal axis (the so-called phase angles) were used as indicators of the gait percents. The speed was estimated according to the distance between the origin and a point on the quasi-circular curves. To estimate different speeds an if-then decision making was required. When speeds and gait percents were estimated, a previously saved look-up table was used to determine the corresponding ankle motion.

Similar to [17], thigh angles and thigh angle integrals were used in [18, 19] to create quasi-circular curves and estimate knee and ankle angles. Next, discrete Fourier transform (DFT) was used to predict the knee and ankle angles as a function of the estimated gait percents. Different sets of phase variables (virtual constraints) were generated for each speed and slope condition. The work was then further extended in [20–22] to take the effects of different speeds and slopes into account. To do so, a basis model was developed which consisted of basis functions (to estimate the joints' angles using DFTs) and task functions that acted as weighting factors to the basis functions.

In [23], seven regression algorithms were investigated to estimate the foot angles at self-selected walking speed using sagittal plane angular velocities and translational accelerations of the foot. In [24], 3D angular velocity and linear acceleration from foot and shank (in total 12 signals) were measured to estimate the sagittal knee and ankle angles. To do so a generalized regression neural network was used. A similar algorithm was used in [25] together with DFT to estimate ankle angles. The algorithm used different parameters such as stride length, cadence, thigh, shank and foot length as inputs. In [26], ankle angles were estimated by using shank angles and angular velocities. To do so, Gaussian regression was utilized to estimate the angles for different individuals walking at several speeds. The work was further extended in [27] to estimate knee angles using thigh angles and angular velocities. The algorithms were tested with motion capture data as well as inertial measurement unit (IMU) data [28, 29]. In [30], it was proposed to use thigh linear accelerations and thigh angles to estimate different walking speeds and gait percents, respectively. Next, using an offline look-up table, the corresponding knee angles were estimated for different walking speeds.

Electromyography (EMG) signals were also used in different studies to estimate knee or ankle angles. In [31] signals from rectus femoris, vastus intermedius, vastus lateralis and semitendinosus were used to continuously estimate the corresponding sagittal knee angles for four subjects walking at a constant pace. The algorithm used a combination of time-domain and frequency domain approaches for feature extraction together with a Levenberg–Marquardt multilayer perceptron neural network for pattern classification. EMG signals from soleus, gastrocnemius and tibialis anterior muscles were used in [32] to predict ankle angles. Two methods were proposed for this purpose. In the first one a biomimetic model was used which required the muscle properties such as isometric length, activation level, muscle stiffness and damping factors. In the second one, a feedforward neural network trained with a standard backpropagation algorithm was used. It was reported that both methods had the ability to predict desired ankle movements. A nonlinear autoregressive neural network was used in [33] to estimate ankle angles. The inputs were EMG signals from ankle flexor and extensor muscles, and the activation functions were tansig and linear function with unit slope. A relatively similar algorithm was also used in [34] to estimate ankle angles through EMG signals from tibialis anterior and gastrocnemius. In [35] a deep belief network together with a back propagation algorithm was used to estimate the hip, knee and ankle angles using EMG signals from ten muscles of the lower extremity (during walking at 0.8, 1, 1.2 m s^{-1}). It was reported that the features extracted from multichannel surface EMG signals using a deep belief network method outperformed a principal components analysis [15] approach. Some studies showed that the inclusion of kinematics data (e.g., angles, velocities) leads to more robustness and accuracy in comparison to using only EMG signals, [36–38].

The current study aims to estimate knee and ankle angles according to the motion of the limb above them (thigh or shank, depending on the joint under study). Therefore, this is different from studies that required, e.g., thigh and shank motions to estimate the knee angles or required shank and foot motions to estimate the ankle angles, [23, 24, 39–42].

Furthermore, our final aim is to continuously map the inputs to the estimated outputs without requiring switching rules, speed estimation, gait percent identification and look-up tables. Methods presented in [17, 18, 20, 22] required such intermediate parameters to finally estimate the corresponding joint angles. Such intermediate parameters were themselves extracted from thigh [18, 20, 22] or shank [17] motions.

In [26, 27], it was proposed to use Gaussian regression in order to circumvent the need for speed and gait percent estimations. To do so, thigh angles and angular velocities were used to directly estimate the knee angles [27]. In [26], shank angles and angular velocities were used to continuously estimate the ankle angles. The results showed that it was possible to directly map the inputs to the outputs, without requiring switching rules, speed estimation, gait percent identification or look-up tables. It was shown,

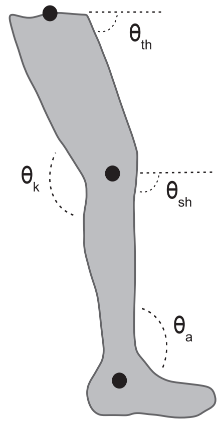

Figure 1. Definition of the thigh angle θ_{th}, knee angle θ_{k}, shank angle θ_{sh} and ankle angle θ_{a}. See also figure 2.

however, that only thigh (shank) angles or only angular velocities were not sufficient to achieve a reasonable estimation performance.

State estimation using minimal sensory inputs, which leads to less marker data and sensory requirement in biomechanical gait analysis as well as design of assistive devices, has been pursued by a number of studies [43–46].

Having the above advancements and limitations in mind, in this study we aimed to estimate the knee/ankle joint angles using only thigh/shank angles. In addition this work aims to estimate those joints' angles without requiring intermediate parameters such as switching rules, speed or gait percent estimations or look-up tables.

To do so, the estimations were performed using nonlinear auto-regressive modeling combined with wavelets theory, and then combining the two in a network.

2. Methods

Thigh and shank angles were used in this study to estimate knee and ankle angles, respectively (in sagittal plane). The definitions of the thigh angle θ_{th}, knee angle θ_{k}, shank angle θ_{sh} and ankle angle θ_{a} are shown in figure 1. The thigh angle is defined as the angle created by the thigh and the horizontal line that passes through the hip joint. Knee angle is the angle between thigh and the shank. Shank angle is defined as the angle created by the shank and the horizontal line that passes through the knee joint. Ankle angle is the angle between the foot and the shank.

In figures 2(A)–(D), thigh angles θ_{th}, knee angles θ_{k}, shank angles θ_{sh}, and ankle angles θ_{a}, are shown together with the mean curves for 21 subjects (11 F, 10 M, 25.4 ± 2.7 (st.d.) (yr), 1.73 ± 0.09 (m), 70.9 ± 11.7 (kg)) walking at 0.5 m s^{-1} (slow), 1 m s^{-1} (moderate) and 1.5 m s^{-1} (fast). The angular values in figures 2(A)–(D) are according to [47].

To estimate knee and ankle angles (estimated outputs $\hat{y}$), the estimation problem was assumed as a dynamic system with input x and output y. The input x is in general a combination of the current and past *external* inputs u (thigh (shank) angles) and past values of outputs y (knee (ankle) angles).

To perform estimations, a nonlinear autoregressive model with exogenous inputs (NARX) [48] was used. The NARX is a modeling technique that in its general form uses past outputs and inputs to estimate the current state of the output [49, 50]. It is specially used for creating a relationship between y and external u and approximating a function according to the available inputs.

To do so, three scenarios were developed. (1) In the first scenario, knee angles θ_{k} (estimated outputs $\hat{y}$) were estimated using thigh angles θ_{th} (external inputs u). (2) In the second scenario, ankle angles θ_{a} were estimated using thigh angles θ_{th}, and (3) in the third scenario ankle angles θ_{a} were estimated using shank angles θ_{sh}.

Assuming a dynamic system [48], the estimated output $\hat{y}$ at the discretized time instance k is related to previous output values (the regressors) $y(k-1), y(k-2), \ldots$ and the external inputs $u(k), u(k-1), \ldots$ as described by

$$\hat{y}(k) = \hat{f}(x(k))$$
$$x(k) = [y(k-1), y(k-2), \ldots, u(k), u(k-1), u(k-2), \ldots], \quad (1)$$

where x is the vector of the regressors and $\hat{f}$ is the estimator function, and $u(k), u(k-1), \ldots$ is $\theta_{\mathrm{th}}(k), \theta_{\mathrm{th}}(k-1), \ldots$, and and $y(k-1), y(k-2), \ldots$ is $\theta_{\mathrm{k}}(k-1), \theta_{\mathrm{k}}(k-2), \ldots$, in case the knee angle is going to be estimated.

The value $\hat{y}$ is an estimation of the desired output y, therefore one would have $y = \hat{f}(x) + e$, where e defines the error of the estimation. Depending on the problem at hand, the number of the past external inputs and outputs in $x(k)$ could vary in order to lead to a reasonable estimation performance [33, 37, 51, 52].

According to the scenarios defined above, the estimated output $\hat{y}$ is θ_{k} or θ_{a} and the external input u is θ_{th} or θ_{sh}, depending on the joint under investigation. Function $\hat{f}$ can be nonlinear functions such as polynomials, wavelets or sigmoids, or a summation of them, e.g., in the form of a network [53, 54].

To define the estimator $\hat{f}$, wavelets [55–57] were used. According to wavelets theory [58], a function can be expressed by the sum of weighted small waves, i.e. the wavelets ψ, that grow and decay through time and should hold certain characteristics. Therefore, the estimator $\hat{f}$ can be expressed as

$$\hat{f}(x) = \Sigma_{i=1}^{L} \omega_i \psi_i(x). \quad (2)$$

The performance of the estimator can be improved by combining the wavelet with the weighted sum of the scaling functions φ, therefore

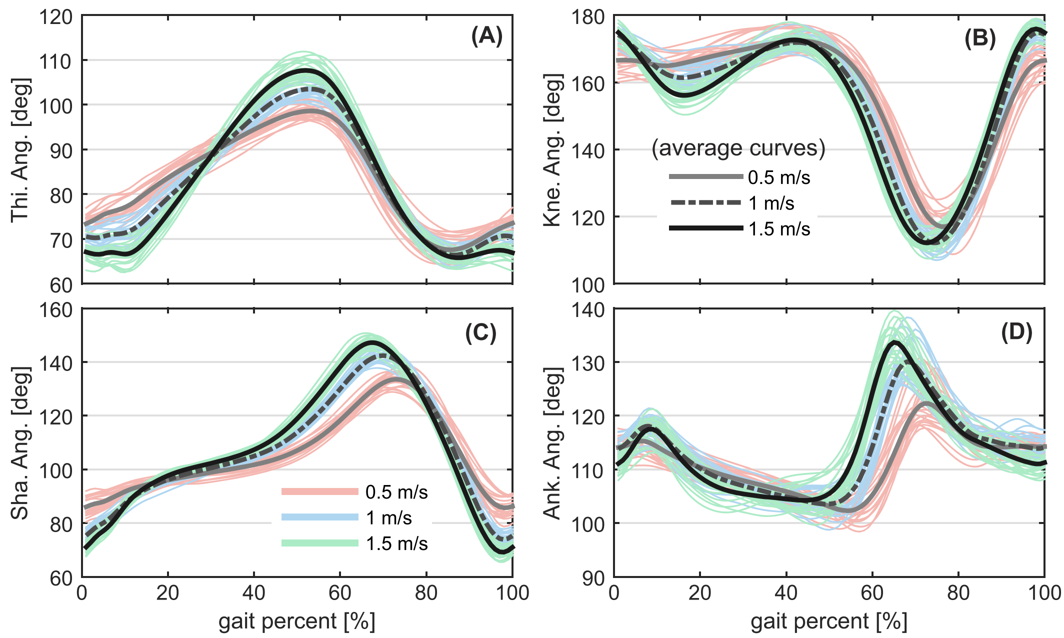

Figure 2. The diagrams of (A): thigh angles θ_{th}, (B): knee angles θ_{k}, (C): shank angles θ_{sh}, and (D): ankle angles θ_{a}, for 21 subjects walking at 0.5, 1 and 1.5 m s^{-1}. The mean curves are in bold for each speed. The values are according to [47].

one would have $\hat{f}(x) = \Sigma_{i=1}^{L_w}\omega_i\psi_i(x) + \Sigma_{k=1}^{L_s}\alpha_k\varphi_k(x)$ [53, 54].

In a way, the weighted sum of the wavelets in equation (2) partially resembles the Fourier series, since the wavelet theory also decomposes a signal into several small waves (the wavelets), however there are fundamental differences. The human gait has a periodic nature which can change through time. Wavelets can capture variations of the system's response both in time and frequency domains [55–57]. Because of their nature, wavelets are able to follow the changes of information in a signal and hence can describe a part of the function with a resolution matched to its scale. This is in contrast to the Fourier basis functions (the never ending sine and cosine functions), which can not describe a function properly when the frequency changes with respect to time (which happens in human locomotion) or when there are singularities at some part of the function to be estimated. Unlike sine and cosine functions, the wavelets decay after a certain amount of time, making them suitable candidates for representing functions with local variations at certain sections of their intervals. Therefore, the wavelets provide more flexibility [58] in comparison to DFT-based approaches [18, 25].

Different candidates of basis functions exist for the wavelets [55, 56, 58]. The basis functions of the wavelets ψ in this study were of the Gaussian derivatives family [59]. The Gaussian-based functions (that have the general form of $g(x) = ae^{-\frac{xx^{\mathrm{T}}}{2}}$, in case the mean $\mu = 0$) are known to be reasonable candidates in studies of joints' motions [60–64]. Therefore, the wavelet function was the second derivative of the Gaussian function expressed as

$$\psi(x) = (d - xx^{\mathrm{T}})e^{-\frac{xx^{\mathrm{T}}}{2}} \tag{3}$$

and the scaling function was the Gaussian function expressed as

$$\varphi(x) = e^{-\frac{xx^{\mathrm{T}}}{2}}. \tag{4}$$

The wavelet ψ grows and decays through time and can be adjusted using the scaling function to approximate functions [53, 54, 59]. In the equations above, L is the number of wavelets (equation (2)) and x^{T} denotes the transpose of x and d is the size (dimension, $1 \times d$) of the input x expressed in equation (1) [55–59].

To expand the capabilities of the wavelet-based NARX modeling to a larger scale, one possible solution is to combine the two in a network. Then the activation functions of the network are the functions expressed in equations (3) and (4) and its inputs are according to equation (1), in which the hidden layer of the network contains the wavelets. The network would be similar to a radial basis function network, however with the main difference that it contains wavelet functions with a multiscale structure [53]. The cost function J (the so-called generalized cross validation) would minimize the errors and the number of the wavelets used through $J = \frac{1}{N}\Sigma_{i=1}^{N}(\hat{f}(x(k)) - y(k))^2 + \frac{2L}{N}\sigma_e^2$, where $y(k)$ are the desired outputs, N is the sample length of the data used for training and σ_e is the variance of the unmodeled differences between the estimated and desired outputs. Full details about wavelet theory used in a network can be found in [53–59].

To train the network, the leave-one-subject-out cross validation procedure was used. In each of the scenarios defined above, the inputs from 20 subjects were used for training, and then the inputs from one remaining subject were used for testing. This was done for each subject individually to estimate his/her joints' angles. The leave-one-subject-out procedure was used to evaluate the generality of the proposed approach. Since each individual subject usually has his/her own individualized gait, the estimation results will be shown in more detail for one of the subjects walking at different speeds.

To evaluate the quality of the estimations, the following performance measures were used:

(a) Root mean square (RMS) errors ($\sqrt{\frac{\sum_{i=1}^{n}(\theta_i-\hat{\theta}_i)^2}{n}}$),
(b) Mean absolute errors (MAEs, $\frac{\sum_{i=1}^{n}|\theta_i-\hat{\theta}_i|}{n}$, and
(c) Correlation coefficient defined by ($\rho_{cc} = \frac{\sum_{i=1}^{n}(\theta_i-\bar{\theta})(\hat{\theta}_i-\bar{\hat{\theta}})}{\sqrt{\sum_{i=1}^{n}(\theta_i-\bar{\theta})^2}\sqrt{\sum_{i=1}^{n}(\hat{\theta}_i-\bar{\hat{\theta}})^2}}$),

where n was the number of the samples, and $\hat{\theta}$ was the estimated joint angle (ankle or knee), and θ was the desired joint angle. These measures were used in different studies, e.g., [23, 24, 65].

A linear version of the auto-regressive model [66] was also investigated (i.e., a linear difference equation). In the linear model, the $\hat{f}$ function is expressed as a linear combination (weighted sum) of the current and past inputs and past outputs expressed in the general form as $\hat{f}(x(k)) = a_0u(k) + a_1u(k-1) + \cdots + b_1y(k-1) + \cdots$, where a_i's and b_i's are scalar values.

According to equation (1), the input $x(k)$ can contain different levels of information. Therefore, we evaluated the performance of the estimator $\hat{f}$ with respect to different components of $x(k)$ (sections 3.1 and 3.2). In addition, it was not of interest to include $y(k-1), y(k-2), \ldots,$ since otherwise the current estimation would be influenced by the previous knee (ankle) angle estimations, and in addition it would make the estimations dependent on an extra source of input. Therefore, it was decided to make the knee/ankle angle estimations dependent only on the *external* inputs u originating from the corresponding limb (i.e., thigh or shank angles, depending on the joint).

3. Results

3.1. Linear vs nonlinear auto-regressive model

The performance of a linear versus a nonlinear auto-regressive model is summarized in table 1 (upper vs lower half).

Table 1 shows the average RMS errors of the knee angle estimations using thigh angles (average values of the subjects at different speeds are reported). The estimations were made using different input variants.

At first, the estimations were performed using only the current value of the external input, i.e., $x(k) = [u(k)]$. Next, the estimations were performed using the current value of the external input, together with its four previous values, i.e., $x(k) = [u(k), u(k-1), u(k-2), u(k-3), u(k-4)]$. For the rest of the investigation, the size of $x(k)$ was increased more as observed in table 1. The table shows that average RMS errors (for all of the speeds) reduced when we increased the inclusion of the past external inputs.

This approach however was not desirable, since average RMS errors converged to a partially meaningful region only when a high number of past values were used. In comparison, a nonlinear auto-regressive model which used only the current external input $u(k)$ (lower half of table 1) resulted in an average RMS error which was only achievable by a high-order linear model. According to this result, the investigation on a linear auto-regressive model was not further pursued.

3.2. Size of the input $x(k)$ in the nonlinear model

The complexity of the estimator can grow undesirably if the input dimension gets too large [53]. Figure 3 shows the change of the RMS errors with respect to different variants of $x(k)$ for the nonlinear model. The RMS errors are for the knee angle estimations using thigh angles, for all of the subjects at different speeds.

At first, in case $x(k) = [u(k)]$, the average RMS errors were very high, e.g., for 0.5 m s^{-1}, the average RMS error was nearly 17.6°. Next, in case of $x(k) = [u(k), u(k-1)]$, the average RMS errors declined to 5.3° (∼70% decrease) for the same speed. Figure 3 also shows that after $x(k) = [u(k), u(k-1)]$, the inclusion of more previous samples did not lead to a very noticeable decrease of the average values. For instance, according to table 1 (lower half), the average RMS errors for $x(k) = [u(k), \ldots, u(k-4)]$ were 5.1°, 3.6°, 4.2° and for $x(k) = [u(k), \ldots, u(k-24)]$ they were 3.8°, 3.2°, 3.4°, for 0.5 m s^{-1}, 1 m s^{-1} and 1.5 m s^{-1}, respectively. In this case, the main difference was seen for 0.5 m s^{-1}, which was about 1.3°.

According to the above finding, a decision was made based on the compromise between the complexity of $x(k)$ and the estimation performance. Therefore, the decision was to go for $x(k) = [u(k), u(k-1)]$ as the type of the input to the wavelet-based nonlinear auto-regressive model, since it was required to have only one past external input in memory. This would also reduce the computational efforts of the algorithm, and according to table 1 (lower half) and figure 3, would not lead to a very bad impact on the estimation quality. Furthermore, table 1 and figure 3 also showed that increasing the size of $x(k)$ did not necessarily lead to a steady decrease of the average RMS errors.

3.3. Results of RMS errors, MAEs and ρ_{cc}

Figure 4 shows the RMS errors (A), MAEs (B), and ρ_{cc} values (C) for different subjects and different speeds. The average results are numerically reported in table 2 as well. The results are for the leave-one-subject-out

Table 1. Comparison of Average RMS errors [°] between a linear auto-regressive model and a nonlinear model for different subjects and different speeds (see also subsection 3.1)

Speeds (m s^{-1})	Components of $x(k)$					
	$[u(k)]$	$[u(k),\ldots,u(k-4)]$	$[u(k),\ldots,u(k-9)]$	$[u(k),\ldots,u(k-14)]$	$[u(k),\ldots,u(k-19)]$	$[u(k),\ldots,u(k-24)]$
(Linear model) 0.5	25.3	22.2	19.8	15.1	11.3	9.6
1	31.7	29.9	26.7	20.6	14.8	10.7
1.5	35.2	33.7	30.1	24.3	18.4	13.6
(Non-linear) 0.5	17.6	5.1	4.4	4.1	4.2	3.8
1	17.1	3.6	3.3	3.1	3.2	3.2
1.5	16	4.2	3.6	3.3	3.6	3.4

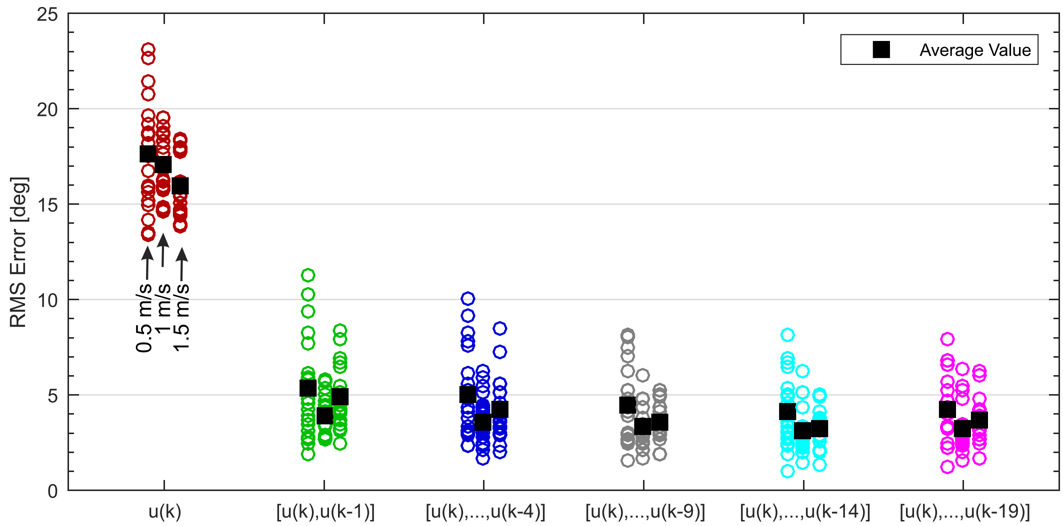

Figure 3. The change of the RMS errors with respect to different variants of $x(k)$, for a nonlinear model. The results are for the knee angle estimations using thigh angles, for different subjects and different speeds, see also subsection 3.2.

Table 2. Comparison of average(±std) RMS errors, MAEs and ρ_{cc} (see also subsection 3.3)

	0.5 m s^{-1}			1 m s^{-1}			1.5 m s^{-1}		
	$\theta_k(\theta_{th})$[a]	$\theta_a(\theta_{th})$	$\theta_a(\theta_{sh})$	$\theta_k(\theta_{th})$	$\theta_a(\theta_{th})$	$\theta_a(\theta_{sh})$	$\theta_k(\theta_{th})$	$\theta_a(\theta_{th})$	$\theta_a(\theta_{sh})$
RMS Er. (°)	5.3(±2.6)	2.6(±0.9)	2.1(±0.7)	3.9(±1.0)	2.9(±1.1)	2.3(±0.8)	4.8(±1.5)	2.7(±1.1)	2.3(±1.0)
MAEs (°)	4(±2.0)	2.1(±0.6)	1.7(±0.5)	3.2(±0.8)	2.3(±0.8)	1.8(±0.5)	3.5(±1.1)	2.2(±0.9)	1.8(±0.8)
ρ_{cc}	0.95(±0.04)	0.90(±0.07)	0.94(±0.04)	0.98(±0.01)	0.93(±0.04)	0.96(±0.02)	0.97(±0.01)	0.95(±0.03)	0.96(±0.02)

[a] $\theta_k(\theta_{th})$ means that θ_k is a function of θ_{th} (scenario 1). A similar definition applies to the other cases. See also figure 4.

cross validation as explained in the Methods section. The blue circles are for the first scenario, where knee angles θ_k were estimated using thigh angles θ_{th}. The red circles show the results for the second scenario, where ankle angles θ_a were estimated using thigh angles θ_{th}, and the green circles are for the third scenario, where ankle angles θ_a were estimated using shank angles θ_{sh}. The black squares show the average values for each part.

3.3.1. Knee angle estimations using thigh angles

The average(±std) RMS errors were 5.3°(±2.6°), 3.9°(±1.0°) and 4.8°(±1.5°) for 0.5 m s^{-1}, 1 m s^{-1} and 1.5 m s^{-1}, respectively. The average MAEs were 4°(±2.0°), 3.2°(±0.8°) and 3.5°(±1.1°) for 0.5 m s^{-1}, 1 m s^{-1} and 1.5 m s^{-1}, respectively. The average ρ_{cc} were 0.95(±0.04), 0.98(±0.01) and 0.97(±0.01) for 0.5 m s^{-1}, 1 m s^{-1} and 1.5 m s^{-1}, respectively.

3.3.2. Ankle angle estimations using thigh angles

The average RMS errors were 2.6°(±0.9°), 2.9°(±1.1°) and 2.7°(±1.1°) for 0.5 m s^{-1}, 1 m s^{-1} and 1.5 m s^{-1}, respectively. The average MAEs were 2.1°(±0.6°), 2.3°(±0.8°) and 2.2°(±0.9°) for 0.5 m s^{-1}, 1 m s^{-1} and 1.5 m s^{-1}, respectively. The average ρ_{cc} were 0.90(±0.07), 0.93(±0.04) and 0.95(±0.03) for 0.5 m s^{-1}, 1 m s^{-1} and 1.5 m s^{-1}, respectively.

3.3.3. Ankle angle estimations using shank angles

The average RMS errors were 2.1°(±0.7°), 2.3°(±0.8°) and 2.3°(±1.0°) for 0.5 m s^{-1}, 1 m s^{-1} and 1.5 m s^{-1}, respectively. The average MAEs were 1.7°(±0.5°), 1.8°(±0.5°) and 1.8°(±0.8°) for 0.5 m s^{-1}, 1 m s^{-1} and 1.5 m s^{-1}, respectively. The average ρ_{cc} were 0.94(±0.04), 0.96(±0.02) and

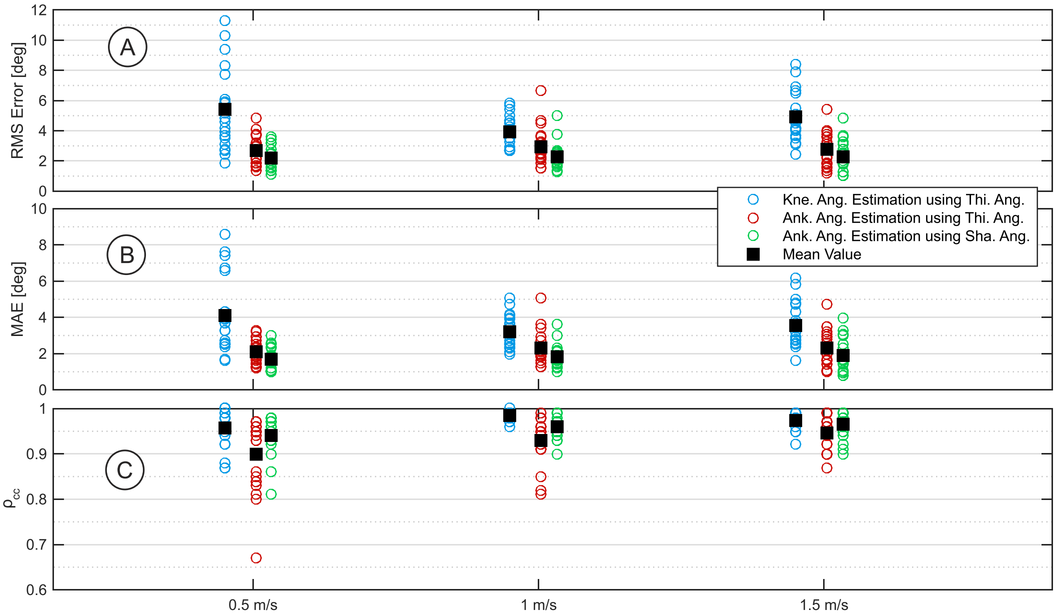

Figure 4. The leave-one-subject-out cross validation results. The RMS errors, MAEs and ρ_{cc} values for knee and ankle angle estimations according to different inputs (θ_{th} or θ_{sh}), subjects and speeds, corresponding to three scenarios defined in Methods section, see also subsection 3.3.

0.96($\pm$0.02) for 0.5 m s^{-1}, 1 m s^{-1} and 1.5 m s^{-1}, respectively.

3.4. Estimated knee and ankle angles vs actual ones

Figure 5 shows the actual and estimated knee and ankle angles for different subjects and speeds, according to the scenarios defined in the methods section. The first column is for the knee angle estimations using thigh angles. The second column is for the ankle angle estimations using thigh angles, and the third column is for the ankle angle estimations using shank angles.

3.5. Average computation time

The average computation time was nearly 0.02 s for each speed (average of all of the subjects). Having in mind 100 gait percents in a gait cycle, accordingly the time required to estimate the joint angle corresponding to a specific gait percent would be nearly 2×10^{-4} s (0.2 ms) on average. The computations were performed using a laptop equipped with an Intel Core i7 CPU and 16 GB of RAM.

For real-time applications, if a prosthetic/orthotic device is working on a frequency of 1 kHz [11, 18], according to the above computation the high-level controller (i.e., the motion planner) would potentially have sufficient time to provide the required estimated value to the low-level controller.

3.6. Case study: performance and estimation quality for one of the subjects

Figure 6, shows the subject-specific results for one individual. For this purpose, an additional male subject (1.77 m, 86 Kg) walked on the treadmill from 0.5 m s^{-1} to 1.5 m s^{-1}, while the thigh angles were recorded using an IMU (Xsens, The Netherlands). To obtain knee angles, another IMU was attached to the shank. Next, the knee angles were calculated using $\theta_k = 180 - (\theta_{sh} - \theta_{th})$. Shank angles were only used to calculate the corresponding synced knee angles and were not required for the estimation task. The figure shows estimated and actual knee angles where estimation was performed using thigh angles. The curves are for slow (0.5 m s^{-1}), moderate (1 m s^{-1}) and fast walking (1.5 m s^{-1}). Here, two gait cycles were used (at each speed) for training. Figure 6 shows test results for five gait cycles of that subject at each speed. The curves show that there is reasonable match between the actual and estimated knee angles (overall RMS error, MAE and ρ_{cc} were 3.7°, 2.4° and 0.98, respectively).

4. Discussions & conclusions

Thigh and shank angles, were used to estimate knee and ankle angles in this study. To do so, a nonlinear auto-regressive model which was combined with wavelets and neural networks was used and the results were shown.

From table 2, it can be observed that the average ρ_{cc} results are relatively lower at 0.5 m s^{-1} in comparison to the other speeds. Furthermore, the standard deviation at this speed was higher in comparison to the other speeds. This potentially might have some connections to the fact that lower walking speed is energetically less efficient [67]. The issue of whether and how kinematics and gait energetics are correlated and affect the estimation performance

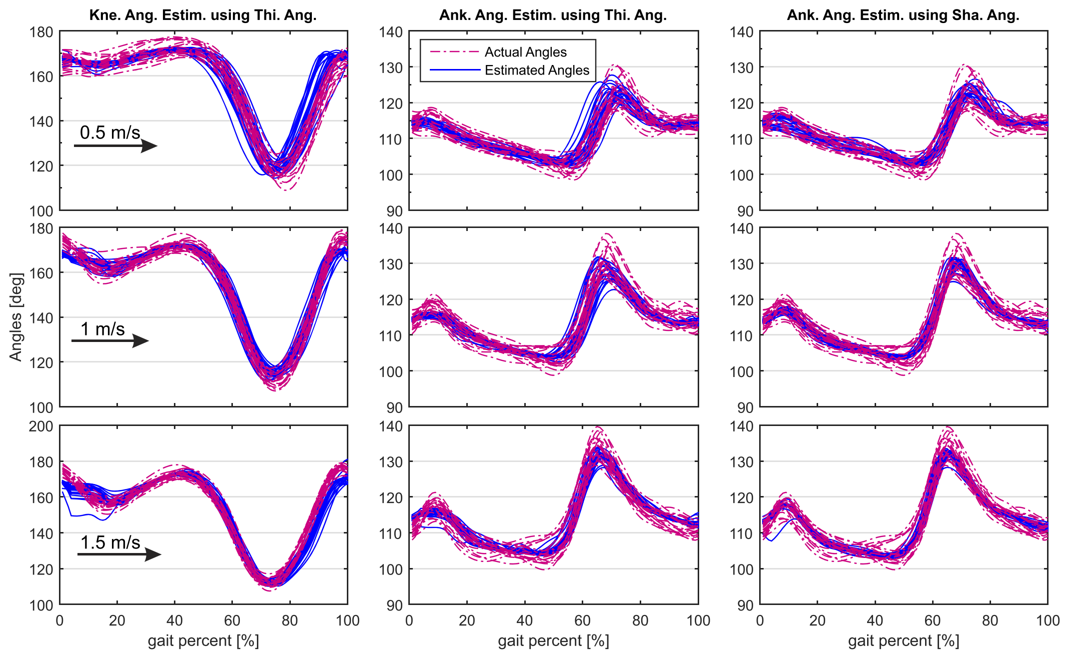

Figure 5. The actual and estimated knee and ankle angles using thigh and shank angles for different subjects and different speeds, according to three scenarios defined in methods section, see also subsection 3.4.

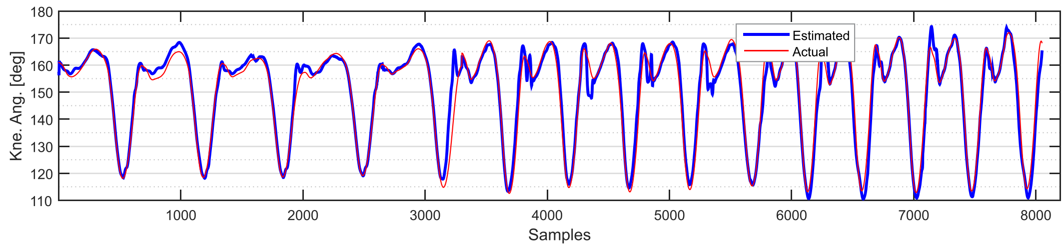

Figure 6. The actual and estimated knee angles (estimation using thigh angles) for one of the subjects at different speeds (for each speed five gait cycles are shown, see subsection 3.6 for more details).

requires further investigations. This can be part of future studies.

For the ankle angle estimations, the average results showed that a better correlation was found between the shank and ankle angles (scenario 3) in comparison to the thigh and ankle angles (scenario 2). This was also reflected in the values of the standard deviations. This potentially can be used as a guideline for designing more efficient motion planners for robotic prostheses, orthoses and exoskeletons.

4.1. Effect of inclusion of the past outputs in $x(k)$

The estimator was also tested when past estimated outputs were included in the input. For $x(k) = [u(k), u(k-1), y(k-1)]$, the mean RMS errors were 11.9°, 8.9°, 8.2° for 0.5, 1 and 1.5 m s^{-1}, respectively. In addition, for $x(k) = [u(k), u(k-1), y(k-1), y(k-2)]$, the mean RMS errors were 19.4°, 17.7°, 18.1°. The above results showed that including previous estimated outputs in $x(k)$ did not necessarily lead to prediction improvement.

4.2. Estimation quality in case of less training

The estimation quality was also evaluated when different training approaches were used. For this purpose, the RMS errors for knee angle estimations using thigh angles are shown in figure 7 for different subjects, speeds, and training approaches.

All of the following estimations were performed using a leave-one-subject-out approach. The far left red circles show the results when full training was implemented in which data from all speeds were used for training. The results are the same as explained in subsection 3.3.1, where the average RMS errors were 5.3°, 3.9° and 4.8° for 0.5 m s^{-1}, 1 m s^{-1} and 1.5 m s^{-1}, respectively.

Case I. In this case, the extrapolation capability of the estimator was studied (green circles). To do so, the training was performed using data from 0.5 and 1 m s^{-1}. Next, the estimator was tested for 0.5, 1 and 1.5 m s^{-1}. In this case, the average RMS errors were 4.4°, 4° and 8.7° for 0.5 m s^{-1}, 1 m s^{-1} and 1.5 m s^{-1}, respectively.

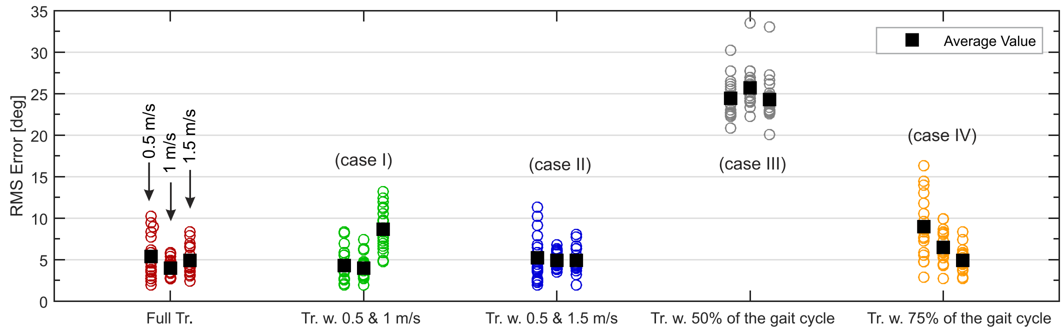

Figure 7. Comparison between RMS errors when different training procedures were used. The results are for the knee angle estimations using thigh angles, for different subjects and different speeds (Tr. w. = Training with). The black squares show the average values, see also subsection 4.2.

Case II. In this case, the interpolation capability of the estimator was studied (blue circles). Therefore, the training was done using data from 0.5 m s^{-1} and 1.5 m s^{-1}. Next, the estimator was tested for 0.5 m s^{-1}, 1 m s^{-1} and 1.5 m s^{-1}. For this case, the average RMS errors were 5.2°, 5° and 4.9° for 0.5, 1 and 1.5 m s^{-1}, respectively.

Case III. In the third case (gray circles), the estimation performance was investigated when for each speed and subject only 50% of data of each gait cycle (i.e., from 1% to 50% of the stride) was used. Next, the estimator was tested for complete gait cycles (i.e., from 1% to 100% of each gait cycle) at 0.5 m s^{-1}, 1 m s^{-1} and 1.5 m s^{-1}. The average RMS errors were 24.4°, 25.7° and 24.4° for 0.5, 1 and 1.5 m s^{-1}, respectively.

Case IV. In this case (orange circles, far right), the estimation performance was investigated when for each speed and subject, 75% of data of each gait cycle (i.e., from 1% to 75% of each gait cycle) was used. Next, the estimator was tested for full gait cycles (i.e., from 1% to 100% of each gait cycle) at 0.5 m s^{-1}, 1 m s^{-1} and 1.5 m s^{-1}. In this case, the average RMS errors were 8.9°, 6.4° and 4.9° for 0.5, 1 and 1.5 m s^{-1}, respectively.

Figure 7 shows that the extrapolation capability of the estimator (case I) performed worse than full training. However, the performance of the interpolation scenario (case II) was relatively close to the full training. In addition, for cases III and IV, it was observed that training with data from only some part of the gait cycle did not lead to an acceptable performance in comparison to the target results (i.e., full training, red circles, far left). Especially, when more data of each gait cycle were used (case IV), the results obviously improved in comparison to case III. It possibly shows that it was important for the estimator to have a knowledge of *the dynamics* of the interactions between a specific limb and its peripheral joint *throughout* the gait cycle.

The results indicate that an efficient training strategy, which includes the data from the lower and upper boundaries, might be potentially sufficient to attain relatively good results. This finding was similar to a previous study [30], where the interpolation approach led to results relatively similar to full-data training for walking speeds estimated from thigh linear accelerations. This potentially can decrease the training time.

4.3. Comparison with other studies

Several studies have estimated knee or ankle angles, using different algorithms and inputs and verified their approach on different sets of subjects. Table 3 reports a summary of different studies in this regard, including current work.

In general both EMG and mechanical (kinematics, kinetics) signals were used for estimations, depending on the study. Some studies additionally used biometric data such as height and age, e.g., [25, 68].

The estimation results of the current study are in the range reported by other studies, noting that only one source of input was used (thigh or shank angles) with a compromised composition of the input $x(k)$ (see subsection 3.3). Figure 3 showed that better results can be expected as well when more previous external inputs u were used, albeit increasing the computational efforts.

4.4. Application in prosthetics, orthotics and exoskeletons

This study aimed to relate the motion of thigh (shank) to the motion of the joint beneath it, knee (ankle) joint. The proposed trajectory estimation approach can be used in motion planning and high-level controlling of humanoids, prosthetics, orthotics and exoskeletons. Since the knee and ankle angles were estimated, those algorithms can be directly used in devices whose actuation mechanisms are stiff, which was the case, e.g., in [18, 72, 73]. In these cases, the desired trajectories of the actuators would be similar to those of the knee or ankle angles.

For real-time applications, thigh or shank angles can be obtained from a thigh- or shank-mounted IMU. Next, the algorithm can be used as a high-level controller to convert those inputs into the estimated

Table 3. Comparison of this study with different studies (see also subsection 4.3 for more information)[a,b].

Study	No. of sources & type of the inputs	Algorithm	No. of subjects	Walk. Speeds	Ave. RMSE (°)	Ave. MAE (°)	Ave. ρ_{cc}
[23] (Ank.)	3| foot ang. vel. & lin. acc.	GRNN	8	moderate	4.7–5.3	3.3–3.7	0.98–0.99
[24] (kne.)						7.1–7.6	0.88–0.89
[24] (Ank.)	12| 3D ang. vel. & lin. acc. from shank & foot	GRNN	8	moderate	—	4.9–5.3	0.70–0.75
[39] (kne.)	12| 3D ang. vel. & acc.from thigh & shank	Rotation matrices	3	moderate	6.8	4.6	0.92
[31] (kne.)	2| EMG signals	MLP NN	4	moderate	—	—	0.59–0.84
[25] (kne.)						5.4	0.97
[25] (Ank.)	6| stride length, cadence, etc.	DFT & GRNN	70	Slow & moderate	—	3.6	0.92
[68] (kne.)						6.95–7.05	
[68] (Ank.)	14| height, mass, gender, etc.	GPR	113	moderate	—	4.20–4.29	—
[35] (kne.)					3.9		0.97
[35] (Ank.)	10| EMG signals	Deep belief NN	6	0.8, 1, 1.2 m s^{-1}	2.4	—	0.95
		NARX net					
[33] (Ank.)	3| EMG signal	(Without wavelets)	3	moderate	1.2–5.4	—	—
[69] (Ank.)	9 | gait events	Feedforward NN	10	moderate	1.2–2		
		NARX net					
[37] (Ank.)	4| EMG & kinema.	(Without wavelets)	10	moderate	2.4	—	0.97
				Very slow to			
[44] (Ank.)	3| EMG signals	Feedforward NN	40	Fast	1.1–2.3	—	0.96–0.99
[70] (kne.)	7| Sacrum acc., vel.,	FF NN	7	1.2, 1.4, 1.8	2.1	—	0.99
[70] (Ank.)	Displa., time				3.3	—	0.99
	7| EMG, $\theta_{th}, \dot{\theta}_{th}$						
[41] (kne.)	$\theta_{sh}, \dot{\theta}_{sh}$	Deep-recurrent NN	11	moderate	2.9	—	—
[20] (kne.)	$2^{+}\|\theta_{th}, \int\theta_{th}$, &	DFT &	10	0.8, 1, 1.2	4.1 [22]	—	—
[20] (Ank.)	Integral reset	Weighted task inclusion			3.4 [22]	—	—
[71] (kne.)	12| lin. acc.& ang. vel.	Deep learning with	27	1.1–3.8	—	2.6–3.7	0.99
[71] (Ank.)	(Ipsilateral shank, thigh)	convolu. & recurr. Layers			—	4.5–5.9	0.95–0.98
[27] (kne.)	2 |$\theta_{th}, \dot{\theta}_{th}$	GPR	23	0.5, 1, 1.5	4.4–6.2	3.3–4.4	—
[26] (Ank.)	2 |$\theta_{sh}, \dot{\theta}_{sh}$	GPR	21	0.5, 1, 1.5	2.1–2.3	—	—
This study (kne.)	1|θ_{th}				3.9–5.3	3.2–4	0.95–0.98
(Ank.)	1|θ_{th}				2.6–2.9	2.1–2.3	0.90–0.95
(Ank.)	1|θ_{sh}	NARX with wavelets	22	0.5, 1, 1.5	2.1–2.3	1.7–1.8	0.94–0.96

[a]GRNN: Generalized regression neural network.
[b]DFT: Discrete Fourier transform.

desired angle of the joint under study. When the desired joint angle is estimated, an error signal can be produced which is the difference between the actual joint angle and the estimated desired one. Next, using appropriate gains, a PD controller (for instance) can be used as a low-level controller to provide the command signal to the actuator (usually a DC motor). Consequently, the motion of the actuator would be a function of the (biological) limb above it. Since the motion of the upper limb (source of the input) is controlled by the human nervous system, this can potentially increase the robustness and reliability of the operation of the prosthetic/orthotic device.

In this study, healthy human data was used for investigating the estimator performance. This is a required step, since healthy human data act as the rational standard and serve as target frame for applications in humanoids, prosthetics, orthotics and exoskeletons. This is an approach that has been adopted by many studies, e.g. [17, 18, 20, 22–24, 39, 41, 44, 68, 71, 74].

Once possible relationships between the functionalities of the lower limbs have been identified, an assistive device can be designed which operates based on the identified rules in human locomotion. Next, the performance can be adapted to the subject-specific needs. To be able to progress in that way, understanding the existing relationships in average healthy human locomotion is an essential step.

Nevertheless, we used amputee data (transfemoral subjects) released publicly by [75], to study the similarity between the inputs that we used in this study (from healthy individuals) and those obtained from the amputees. To do so, the amputees' thigh angles were compared with average healthy individuals data obtained from [47]. The correlation coefficient were 0.93–0.99, 0.95–0.99, and 0.93–0.98 for slow, moderate and fast walking speeds, for ten amputee subjects (23–65 years old). The values showed that there was acceptable correspondence (similarity) between these amputee data and healthy individual data.

This shows that the amputee thigh angles can be potentially used for the estimation of the corresponding knee angles. Since those amputees' inputs (i.e., thigh angles) were similar to the healthy data, the estimator would potentially generate the corresponding estimated knee angles in the region of and similar to the curves seen in figure 5. However, to make a more robust conclusion, further comprehensive investigations will be required to evaluate how the proposed algorithm would perform for different amputee subjects and when used in clinical applications.

In addition, future work should involve investigating the performance of the proposed estimation algorithm for other gaits such as ascending and descending stairs and/or slopes.

Acknowledgment

The authors would like to express their gratitude to Lauflabor, Technical University of Darmstadt, Germany, and the lab director Professor Dr A Seyfarth, for providing the angles data. This work was supported by the Grant from the Bundesministerium für Bildung und Forschung (BMBF, INOPRO-16SV7657).

Data availability statement

The data that support the findings of this study are available upon reasonable request from the authors.

ORCID iDs

Mahdy Eslamy https://orcid.org/0000-0002-1822-7225

References

[1] Borghese N A, Bianchi L and Lacquaniti F 1996 Kinematic determinants of human locomotion *J. Physiol.* **494** 863–79
[2] Whittle M W 2003 *Gait Analysis: An Introduction* (Oxford: Heinemann)
[3] Frigo C, Crenna P and Jensen L M 1996 Moment-angle relationship at lower limb joints during human walking at different velocities *J. Electromyogr. Kinesiol.* **6** 177–90
[4] Sup F, Bohara A and Goldfarb M 2008 Design and control of a powered transfemoral prosthesis *Int. J. Robot. Res.* **27** 263–73
[5] Varol H A, Sup F and Goldfarb M 2010 Multiclass real-time intent recognition of a powered lower limb prosthesis *IEEE Trans. Biomed. Eng.* **57** 542–51
[6] Sup F, Varol H A and Goldfarb M 2010 Upslope walking with a powered knee and ankle prosthesis: initial results with an amputee subject *IEEE Trans. Neural Syst. Rehabil. Eng.* **19** 71–8
[7] Culver S, Bartlett H, Shultz A and Goldfarb M 2018 A stair ascent and descent controller for a powered ankle prosthesis *IEEE Trans. Neural Syst. Rehabil. Eng.* **26** 993–1002
[8] Ramezani A, Hurst J W, Akbari Hamed K and Grizzle J W 2014 Performance analysis and feedback control of atrias, a three-dimensional bipedal robot *J. Dyn. Syst. Meas. Control* **136** 021012
[9] Kawaharazuka K, Makino S, Kawamura M, Asano Y, Okada K and Inaba M 2018 A method of joint angle estimation using only relative changes in muscle lengths for tendon-driven humanoids with complex musculoskeletal structures *IEEE/RAS Int. Conf. Humanoid Robots (Humanoids)* pp 1128–35
[10] Riener R, Lünenburger L, Maier I C, Colombo G and Dietz V 2010 Locomotor training in subjects with sensori-motor deficits: an overview of the robotic gait orthosis lokomat *J. Healthcare Eng.* **1** 197–216
[11] Ward J, Sugar T, Boehler A, Standeven J and Engsberg J R 2011 Stroke Survivors'gait adaptations to a powered ankle–foot orthosis *Adv. Robot.* **25** 1879–901
[12] Grimes D L, Flowers W C and Donath M 1977 Feasibility of an active control scheme for above knee prostheses *J. Biomech. Eng.* **99** 215–21
[13] Grimes D L 1979 An active multi-mode above knee prosthesis controller PhD Dissertation Massachusetts Institute of Technology

[14] Vallery H, Van Asseldonk E H F, Buss M and Van Der Kooij H 2009 Reference trajectory generation for rehabilitation robots: complementary limb motion estimation *IEEE Trans. Neural Syst. Rehabil. Eng.* **17** 23–30

[15] Jolliffe I 2002 *Principal Component Analysis* 2nd edn (New York: Springer)

[16] Winter D A 2009 *Biomechanics and Motor Control of Human Movement* (New York: Wiley)

[17] Holgate M, Sugar T and Bohler A 2009 A novel control algorithm for wearable robotics using phase plane invariants *IEEE Int. Conf. on Robotics and Automation (ICRA)* pp 3845–50

[18] Quintero D, Villarreal D J, Lambert D J, Kapp S and Gregg R D 2018 Continuous-phase control of a powered knee–ankle prosthesis: amputee experiments across speeds and inclines *IEEE Trans. Robot.* **34** 686–701

[19] Villarreal D J and Gregg R D 2020 Controlling a powered transfemoral prosthetic leg using a unified phase variable *Wearable Robotics* (Amsterdam: Elsevier) pp 487–506

[20] Embry K R, Villarreal D J, Macaluso R L and Gregg R D 2018 Modeling the kinematics of human locomotion over continuously varying speeds and inclines *IEEE Trans. Neural Syst. Rehabil. Eng.* **26** 2342–50

[21] Embry K R and Gregg R D 2020 Analysis of continuously varying kinematics for prosthetic leg control applications *IEEE Trans. Neural Syst. Rehabil. Eng.* **29** 262–72

[22] Reznick E, Embry K and Gregg R D 2020 Predicting individualized joint kinematics over a continuous range of slopes and speeds *IEEE RAS/EMBS Int. Conf. for Biomedical Robotics and Biomechatronics (BioRob)* pp 666–72

[23] Goulermas J Y, Howard D, Nester C J, Jones R K and Ren L 2005 Regression techniques for the prediction of lower limb kinematics *J. Biomech. Eng.* **127** 1020–4

[24] Findlow A, Goulermas J Y, Nester C, Howard D and Kenney L P J 2008 Predicting lower limb joint kinematics using wearable motion sensors *Gait Posture* **28** 120–6

[25] Luu T P, Low K H, Qu X, Lim H B and Hoon K H 2014 An individual-specific gait pattern prediction model based on generalized regression neural networks *Gait Posture* **39** 443–8

[26] Eslamy M and Alipour K 2019 Synergy-based gaussian process estimation of ankle angle and torque: conceptualization for high level controlling of active robotic foot prostheses/orthoses *ASME J. Biomech. Eng.* **141** 021002

[27] Eslamy M, Oswald F and Schilling A F 2020 Estimation of knee angles based on thigh motion: a functional approach and implications for high-level controlling of active prosthetic knees *IEEE Control Systems* **40** 49–61

[28] Eslamy M and Schilling A F 2018 A conceptual high level controller to walk with active foot prostheses/orthoses *IEEE Int. Conf. on Biomedical Robotics and Biomechatronics (Biorob)* pp 1224–9

[29] Eslamy M, Oswald F and Schilling A F 2020 Motion planning for active prosthetic knees *IEEE RAS/EMBS Int. Conf. for Biomedical Robotics and Biomechatronics (BioRob)* (Piscataway, NJ: IEEE) pp 465–70

[30] Eslamy M, Oswald F and Schilling A 2020 Mapping thigh motion to knee motion: implications for motion planning of active prosthetic knees *IEEE/RSJ Int. Conf. on Intelligent Robots and Systems (IROS)*

[31] Delis A L, Carvalho J L A, Da Rocha A F, Ferreira R U, Rodrigues S S and Borges G A 2009 Estimation of the knee joint angle from surface electromyographic signals for active control of leg prostheses *Physiol. Meas.* **30** 931

[32] Au S, Bonato P and Herr H 2005 An emg-position controlled system for an active ankle-foot prosthesis: an initial experimental study *IEEE Int. Conf. on Rehabilitation Robotics ICORR* pp 375–9

[33] Farmer S, Silver-Thorn B, Voglewede P and Beardsley S A 2014 Within-socket myoelectric prediction of continuous ankle kinematics for control of a powered transtibial prosthesis *J. Neural Eng.* **11** 056027

[34] Mamikoglu U, Andrikopoulos G, Nikolakopoulos G, Röijezon U, Pauelsen M and Gustafsson T 2016 Electromyography based joint angle estimation and control of a robotic leg *IEEE Int. Conf. on Biomedical Robotics and Biomechatronics* pp 182–7

[35] Chen J, Zhang X, Cheng Y and Xi N 2018 Surface EMG based continuous estimation of human lower limb joint angles by using deep belief networks *Biomed. Signal Process. Control* **40** 335–42

[36] Huang H, Zhang F, Hargrove L J, Dou Z, Rogers D R and Englehart K B 2011 Continuous locomotion-mode identification for prosthetic legs based on neuromuscular–mechanical fusion *IEEE Trans. Biomed. Eng.* **58** 286–2875

[37] Gupta R, Dhindsa I S and Agarwal R 2020 Continuous angular position estimation of human ankle during unconstrained locomotion *Biomed. Signal Process. Control* **60** 101968

[38] Young A J, Kuiken T A and Hargrove L J 2014 Analysis of using emg and mechanical sensors to enhance intent recognition in powered lower limb prostheses *J. Neural Eng.* **11** 056021

[39] Takeda R, Tadano S, Natorigawa A, Todoh M and Yoshinari S 2009 Gait posture estimation using wearable acceleration and gyro sensors *J. Biomech.* **42** 2486–94

[40] Yun X, Calusdian J, Bachmann E R and McGhee R B 2012 Estimation of human foot motion during normal walking using inertial and magnetic sensor measurements *IEEE Trans. Instrum. Meas.* **61** 2059–72

[41] Huang Y, He Z, Liu Y, Yang R, Zhang X, Cheng G, Yi J, Ferreira J P and Liu T 2019 Real-time intended knee joint motion prediction by deep-recurrent neural networks *IEEE Sens. J.* **19** 11503–9

[42] Oubre B, Daneault J-F, Boyer K, Kim J H, Jasim M, Bonato P and Lee S I 2020 A simple low-cost wearable sensor for long-term ambulatory monitoring of knee joint kinematics *IEEE Trans. Biomed. Eng.* **67** 3483–90

[43] Khademi G and Simon D 2021 Toward minimal-sensing locomotion mode recognition for a powered knee–ankle prosthesis *IEEE Trans. Biomed. Eng.* **68** 967–79

[44] Keles A D and Yucesoy C A 2020 Development of a neural network based control algorithm for powered ankle prosthesis *J. Biomech.* **113** 110087

[45] Hahn M E and O'Keefe K B 2008 A neural network model for estimation of net joint moments during normal gait *J. Musculoskelet. Res.* **11** 117–26

[46] Osateerakun P, Barton G, Foster R, Bennett S and Lakshminarayan R 2018 P 037 - prediction of moments from movements without force platforms using artificial neural networks: a pilot test *Gait Posture* **65** 299–300

[47] Lipfert S 2010 *Kinematic and Dynamic Similarities between Walking and Running* (Hamburg: Verlag Dr. Kovac)

[48] Isermann R and Münchhof M 2010 *Identification of Dynamic Systems: An Introduction with Applications* (Berlin: Springer)

[49] Sjoberg J, Zhang Q, Ljung L, Benveniste A, Delyon B, Glorennec P, Hjalmarsson H and Juditsky A 1997 Nonlinear black-box modeling in system-identification-a unified overview-reply *Automatica* **33** 1198

[50] Juditsky A, Hjalmarsson H, Benveniste A, Delyon B, Ljung L, SjÖberg J and Zhang Q 1995 Nonlinear black-box models in system identification: mathematical foundations *Automatica* **31** 1725–50

[51] Tsungnan Lin T, Horne B G, Tino P and Giles C L 1996 Learning long-term dependencies in narx recurrent neural networks *IEEE Trans. Neural Netw.* **7** 1329–38

[52] Boussaada Z, Curea O, Remaci A, Camblong H and Mrabet Bellaaj N 2018 A nonlinear autoregressive exogenous (narx) neural network model for the prediction of the daily direct solar radiation *Energies* **11** 620

[53] Qinghua Zhang Q 1997 Using wavelet network in nonparametric estimation *IEEE Trans. Neural Netw.* **8** 227–36

[54] Zhang Q and Benveniste A 1992 Wavelet networks *IEEE Trans. Neural Netw.* **3** 889–98

[55] Daubechies I 1990 The wavelet transform, time-frequency localization and signal analysis *IEEE Trans. Inform. Theor.* **36** 961–1005

[56] Mallat S G 1989 A theory for multiresolution signal decomposition: the wavelet representation *IEEE Trans. Pattern Anal. Machine Intell.* **11** 674–93

[57] Daubechies I 1988 Orthonormal bases of compactly supported wavelets *Commun. Pure Appl. Math.* **41** 909–96

[58] Daubechies I 1992 *Ten Lectures on Wavelets* (Philadelphia, PA: SIAM)

[59] Kugarajah T and Qinghua Zhang Q 1995 Multidimensional wavelet frames *IEEE Trans. Neural Netw.* **6** 1552–6

[60] Chen S, Cowan C F and Grant P M 1992 Orthogonal least squares learning algorithm for radial basis function networks *IEEE Trans. Neural Netw.* **2** 302–9

[61] Popovic D and Jonic S 1998 Determining synergy between joint angles during locomotion by radial basis function neural networks *IEEE Eng. Med. Biol. Soc.* **5** 2301–4

[62] Jonic S, Jankovic T, Gajic V and Popvic D 1999 Three machine learning techniques for automatic determination of rules to control locomotion *IEEE Trans. Biomed. Eng.* **46** 300–10

[63] Milovanovic I 2008 Radial basis function (rbf) networks for improved gait analysis *IEEE Symp. Neural Network Applications in Electrical Engineering* pp 129–32

[64] Thor M, Kulvicius T and Manoonpong P 2020 Generic neural locomotion control framework for legged robots *IEEE Trans. Neural Netw. Learn. Syst.* **32** 4013–25

[65] Bogey R A and Barnes L A 2017 An emg-to-force processing approach for estimating *in vivo* hip muscle forces in normal human walking *IEEE Trans. Neural Syst. Rehabil. Eng.* **25** 1172–9

[66] Ljung L 1999 System identification *Wiley Encyclopedia of Electrical and Electronics Engineering* vol 1–19 (New York: Wiley)

[67] Eslamy M 2014 Emulation of ankle function for different gaits through active foot prosthesis: actuation concepts, control and experiments PhD Dissertation Technische Universität Darmstadt, Germany

[68] Yun Y, Kim H-C, Shin S Y, Lee J, Deshpande A D and Kim C 2014 Statistical method for prediction of gait kinematics with gaussian process regression *J. Biomech.* **47** 186–92

[69] Sivakumar S, Gopalai A A, Lim K H and Gouwanda D 2019 Artificial neural network based ankle joint angle estimation using instrumented foot insoles *Biomed. Signal Process. Control* **54** 101614

[70] Lim H, Kim B and Park S 2020 Prediction of lower limb kinetics and kinematics during walking by a single imu on the lower back using machine learning *Sensors* **20** 130

[71] Hernandez V, Dadkhah D, Babakeshizadeh V and Kulić D 2021 Lower body kinematics estimation from wearable sensors for walking and running: a deep learning approach *Gait Posture* **83** 185–93

[72] Elery T, Rezazadeh S, Nesler C and Gregg R D 2020 Design and validation of a powered knee–ankle prosthesis with high-torque, low-impedance actuators *IEEE Trans. Robot.* **36** 1649–68

[73] Azocar A F, Mooney L M, Duval J-F, Simon A M, Hargrove L J and Rouse E J 2020 Design and clinical implementation of an open-source bionic leg *Nat. Biomed. Eng.* **4** 941–53

[74] He Huang H, Kuiken T A and Lipschutz R D 2009 A strategy for identifying locomotion modes using surface electromyography *IEEE Trans. Biomed. Eng.* **56** 65–73

[75] Hood S, Ishmael M K, Gunnell A, Foreman K and Lenzi T 2020 A kinematic and kinetic dataset of 18 above-knee amputees walking at various speeds *Sci. Data* **7** 1–8